Squeezed state dynamics of kicked quantum systems

Bambi Hu,[1,2] Baowen Li,[1] Jie Liu,[1,3] and Ji-Lin Zhou[1,4]
[1]*Department of Physics and Centre for Nonlinear Studies, Hong Kong Baptist University, Hong Kong, China*
[2]*Department of Physics, University of Houston, Houston, Texas 77204*
[3]*Institute of Applied Physics and Computational Mathematics, P.O. Box 8009, 100088 Beijing, China*
[4]*Department of Astronomy, Nanjing University, 210093 Nanjing, China*
(Received 9 February 1998; revised manuscript received 20 April 1998)

We study kicked quantum systems by using the squeezed state approach. Taking the kicked quantum harmonic oscillator as an example, we demonstrate that chaos in an underlying classical system can be enhanced as well as suppressed by quantum fluctuations. Three different energy diffusions are observed in the kicked quantum harmonic oscillator, namely, localization, linear diffusion, and quadratic diffusion. [S1063-651X(98)06508-8]

PACS number(s): 05.45.+b, 03.65.Sq, 05.40.+j

I. INTRODUCTION

A squeezed state is a generalized coherent state, which has a wide application in many branches of physics such as quantum optics, high energy physics, etc. Recent years have witnessed a growing application of the squeezed state to the field of nonlinear dynamics and chaos [1–12]. Since the squeezed state approach is a kind of approximation of quantum mechanics, it is called a *semiquantum approach* by people in this community. The time evolution of expectation values and fluctuations of the squeezed state is thus named *semiquantum dynamics*, or *squeezed state dynamics*.

The main purpose of the squeezed state approach is to study how quantum fluctuations manifest themselves on classical trajectories. This approach starts directly from quantum systems with no reference to classical limit. In fact, it has been shown [5] that the squeezed state dynamics exits even for systems without a well-defined classical dynamics. Generally, the squeezed state approach simplifies the quantum version, and provides a complementary way to the semiclassical method. In some special cases (unfortunately, we still do not know under what kind of conditions), it gives us better results than the semiclassical method [1–5,7,8]. Therefore, in addition to the semiclassical approach, the squeezed state approach is also a very useful tool to study the problem of classical-quantum correspondence.

The squeezed state approach has proven to be very successful in studying dynamical systems ranging from integrable to many-body nonintegrable systems. Among many others, we name just a few examples here. In calculating the ground state energy for quantum system with potential $V(q)=-V_0/\cosh^2\alpha q$, Tsui [8] discovered that the ground state energy obtained by the squeezed state approach is much closer to the exact ground state energy than that obtained from the WKB method. More recently, Pattanayak and Schieve [11] applied this approach to a classically chaotic system, for which the WKB method completely fails. They have successfully calculated low-lying eigenenergies which agree within a few percent with the pure quantum (numerical) results. In addition to the ground state and/or lower excited state energies, the squeezed state approach can provide a way to obtain correct eigenfunctions. For instance, in applying the squeezed state approach to a harmonic oscillator, we can obtain not only the eigenenergies but also the eigenfunctions (including the ground state) exactly, as we shall see in Appendix A, whereas the semiclassical method fails to yield the exact eigenfunctions. As a further example of many-body systems, we would like to mention that we have used the squeezed state approach to the one-dimensional quantum Frenkel-Kontoroval model [13], which is a nontrivial many-body, nonintegrable system. Our results show that the squeezed state approach very nicely captures the feature of the quantum effect, namely, the standard map which, determining the coordinates of the classical ground state, is renormalized to an effective sawtooth map in the quantum case. The squeezed state results agree well with that of the quantum Monte Carlo method [13].

In this paper, we would like to apply the squeezed state to study generic behaviors of kicked quantum systems. It is well known that, in the development of quantum chaos, kicked quantum systems play a very important role. Prototypes of these kicked systems are the kicked rotator and kicked harmonic oscillator (KHO). They represent two different classes of dynamical systems. On the one hand, the kicked rotator obeys the Kolmogorov-Arnold-Moser (KAM) theorem. Classically, as the kick strength increases, invariant curves gradually break up. When the kick strength exceeds a critical value of $K_c=0.9716\ldots$, the last invariant curve disappears, and bounded chaos turns into global chaos, characterized by unbounded diffusion in the momentum direction [14]. Quantum mechanically, the diffusion follows the classical one only up to a certain time, after which it is completely suppressed, thus leading to dynamical localization [15]. This phenomenon was connected to the Anderson localization [16], and was confirmed experimentally [17].

On the other hand, since a harmonic oscillator is a degenerate system, the KHO model is out of the framework of the KAM theorem; that is, diffusion can occur along stochastic webs for any small kick strength. As a matter of fact, the KHO model is not a toy model; it stems from a real physical system. It describes a charged particle moving in a magnetic field, and under the disturbance of a wave packet [18]. It has $1\frac{1}{2}$ degrees of freedom. Classically, it depends on the ratio

between frequency of the harmonic oscillator and that of the external kicks [see Eq. (34)]. This system displays abundant structures in phase space such as crystal, quasicrystal, and stochastic webs [18,19]. Moreover, since the phase space of the KHO is unbounded and cannot be reduced to a cylinder, as in the case of the kicked rotator model, numerical investigation of the quantum KHO is much more difficult than that of the kicked rotator model. Therefore, contrary to the kicked rotator, only a few attempts have been made in the quantum KHO [20–24]. A general picture about the quantum behavior of the KHO is still lacking.

In this paper, using the squeezed state approach, we are able to obtain the diffusion behavior of the quantum KHO model not only numerically but also analytically. The paper is organized as follows. In Sec. II, we give a brief introduction of the squeezed state approach for purposes of self-containment. In Sec. III, by using the KHO model, we shall demonstrate that quantum fluctuations will enhance chaos at a small perturbation regime, whereas it will suppress chaotic diffusion at a large perturbation regime. In Sec. IV, we shall study the diffusion and localization phenomena. In Sec. V, comparisons between the squeezed state results and the very few available quantum results will be given. We shall conclude our paper with discussions and remarks in Sec. VI. In Appendix A, we apply this approach to quantize the harmonic oscillator, which exactly yields eigenenergies and eigenfunctions. In Appendix B, we outline our procedure of the pure quantum computation for KHO in some special cases.

II. SQUEEZED STATE APPROACH

The squeezed state approach starts from the time-dependent variational principle (TDVP) formulation

$$\delta \int dt \langle \Psi(t)| i\hbar \frac{\partial}{\partial t} - \hat{H} |\Psi(t)\rangle = 0. \tag{1}$$

Variation with respect to $\langle \Psi(t)|$ and $|\Psi(t)\rangle$ gives rise to the Schrödinger equation, and its complex conjugate (see, e.g., Ref. [25]), respectively. The true solution may be approximated by restricting the choice of states to a subspace of the full Hilbert space, and finding the path along which the above equation is satisfied within this subspace. In the squeezed state approach, the squeezed coherent state is chosen as $|\Psi(t)\rangle$. In this manner, as we shall see below, in addition to the dynamics of centroid of wave packet, we will also have equations of motion for the fluctuations, i.e., the spread of wave packet. Therefore, this approach enables us to study the effects of the quantum fluctuations on dynamical behavior.

The squeezed state is defined by the ordinary harmonic oscillator displacement operator $\mathcal{D}(\alpha)$ acting on a squeezed vacuum state $\mathcal{S}(\beta)|0\rangle$:

$$|\alpha\beta\rangle = \mathcal{D}(\alpha)\mathcal{S}(\beta)|0\rangle,$$

$$\mathcal{D}(\alpha) = \exp(\alpha \hat{a}^+ - \alpha^* \hat{a}), \tag{2}$$

$$\mathcal{S}(\beta) = \exp[\tfrac{1}{2}(\beta \hat{a}^{+2} - \beta^* \hat{a}^2)].$$

$\hat{a}^+$ and $\hat{a}$ are boson creation and annihilation operators which satisfy the canonical commutation relation $[\hat{a}, \hat{a}^+] = 1$. The coherent state is just operator $\mathcal{D}$ acting on the vacuum state $|0\rangle$,

$$|\alpha\rangle = \mathcal{D}(\alpha)|0\rangle. \tag{3}$$

In terms of the number eigenstate $|n\rangle$, the coherent state can be written as

$$|\alpha\rangle = \exp\left(-\frac{1}{2}|\alpha|^2\right) \sum_{n=0}^{\infty} \frac{\alpha^n}{\sqrt{n!}} |n\rangle. \tag{4}$$

α is eigenvalue of creation operator, i.e.,

$$\hat{a}|\alpha\rangle = \alpha|\alpha\rangle. \tag{5}$$

Denoting

$$\alpha = |\alpha| e^{i\eta}, \tag{6}$$

and taking the integral over angle η from 0 to 2π on both sides of Eq. (4), we obtain the number eigenstate expressed in terms of the coherent state,

$$|n\rangle = \frac{1}{2\pi} \exp\left(\frac{1}{2}|\alpha|^2\right) |\alpha|^{-n} \sqrt{n!} \int_0^{2\pi} d\eta\, e^{-in\eta} |\alpha\rangle. \tag{7}$$

The coordinate and momentum operators are defined as

$$\hat{p} = i\sqrt{\frac{\hbar}{2}}(\hat{a}^+ - \hat{a}),$$

$$\hat{q} = \sqrt{\frac{\hbar}{2}}(\hat{a}^+ + \hat{a}). \tag{8}$$

Thus we have expectation values and variances

$$p \equiv \langle \Psi(t)|\hat{p}|\Psi(t)\rangle = i\sqrt{\frac{\hbar}{2}}(\alpha^* - \alpha),$$

$$q \equiv \langle \Psi(t)|\hat{q}|\Psi(t)|\rangle = \sqrt{\frac{\hbar}{2}}(\alpha^* + \alpha), \tag{9}$$

$$\Delta q^2 \equiv \langle \Psi(t)|(\hat{q} - q)^2|\Psi(t)|\rangle = \hbar G,$$

$$\Delta p^2 \equiv \langle \Psi(t)|(\hat{p} - p)^2|\Psi(t)|\rangle = \hbar\left(\frac{1}{4G} + 4\Pi^2 G\right). \tag{10}$$

The canonical coordinates (G, Π) were introduced by Jakiw and Kerman [26] for the quantum fluctuations, and its relation with β in Eq. (2) is [5,8]

$$G \equiv \frac{1}{2}\left|\cosh|\beta| + \frac{\beta}{|\beta|}\sinh|\beta|\right|^2,$$

$$\Pi \equiv \frac{i}{2}\frac{\beta^* - \beta}{|\beta|}\frac{\sinh|\beta|\cosh|\beta|}{\left|\cosh|\beta| + \frac{\beta}{|\beta|}\sinh|\beta|\right|^2}. \tag{11}$$

In the framwork of the squeezed state, the Heisenberg uncertainty relation becomes

$$\Delta q \Delta p = \frac{\hbar}{2}\sqrt{1 + 16G^2\Pi^2} \geqslant \frac{\hbar}{2}. \tag{12}$$

In fact, the squeezed state $|\alpha\beta\rangle$ is equivalent to the Gaussian-type state [7]

$$|\Psi(t)\rangle \equiv \frac{1}{(2G)^{1/4}}\exp\left(\frac{i}{\hbar}(p\hat{q} - q\hat{p})\right)\exp\left(\frac{1}{2\hbar}\Omega\hat{q}^2\right)|0\rangle$$
$$= e^{-i\psi}|\alpha\beta\rangle, \tag{13}$$

where

$$\Omega = 1 - \frac{1}{2G} + 2i\Pi,$$

$$e^{-2i\psi} = \frac{1}{\sqrt{G}}\left(\cosh|\beta| + \frac{\beta}{|\beta|}\sinh|\beta|\right). \tag{14}$$

From the TDVP, we obtain dynamical equations for expectation values and quantum fluctuations,

$$\dot{q} = \frac{\partial H}{\partial p}, \quad \dot{p} = -\frac{\partial H}{\partial q}, \tag{15}$$

$$\hbar\dot{G} = \frac{\partial H}{\partial \Pi}, \quad \hbar\dot{\Pi} = -\frac{\partial H}{\partial G}, \tag{16}$$

which are canonical equations of motion. The dot denotes the time derivative, and the Hamiltonian function H is given by definition

$$H \equiv \langle\Psi(t)|\hat{H}|\Psi(t)\rangle. \tag{17}$$

These equations (15), and 16) give us a simple and clear picture about the motion of the expectation values as well as the evolution of the quantum fluctuations, which are responsible for quantum diffusion. If the Hamiltonian consists of separate kinetic and potential terms such as

$$\hat{H} = \tfrac{1}{2}\hat{p}^2 + V(\hat{q}), \tag{18}$$

then the Hamiltonian function can be written as

$$H = \frac{1}{2}p^2 + V(q) + \hbar\left(\frac{1}{8G} + 2G\Pi^2\right)$$
$$+ \left\{\exp\left[\frac{\hbar}{2}G\left(\frac{\partial}{\partial q}\right)^2\right] - 1\right\}V(q). \tag{19}$$

In the limit of $\hbar = 0$, this Hamiltonian function reduces to the classical Hamiltonian.

Initial conditions

In order to solve the equations of motion (15) and (16), appropriate initial condition for variables (q,p) and (G,Π) should be posed. In principle, the initial condition must be physically meaningful. Thus the following two conditions are generally selected.

(1) *Minimum uncertainty*. The initial state $|\Psi(t_0)\rangle$ should satisfy the condition of minimum uncertainty. Because G_0 is always larger than zero, from the uncertainty principle [Eq. (12)], we have

$$\Pi(t_0) = 0. \tag{20}$$

(2) *Least quantum effect*. We need to determine the initial value of G. This can be achieved by requesting minimization of H with respect to G, i.e.,

$$\frac{\partial H}{\partial G} = 0, \quad \frac{\partial^2 H}{\partial G^2} > 0. \tag{21}$$

For instance, for a harmonic oscillator (Appendix A) we have $G(t_0) = 1/2\omega_0$.

III. ENHANCEMENT AND SUPPRESSION OF CHAOS

In this section, we would like to discuss the effect of quantum fluctuations on classical chaos. It is commonly argued that quantum fluctuations suppress classical chaos due to interference, while enhancing chaos due to tunneling. This is a rather qualitative argument. With the help of the squeezed state approach, we are able to do a quantitative analysis of quantum fluctuations.

Up to now, there have been only a few works on this issue. In some models, suppression of chaos comes about, while in others enhancement takes place. Zhang and coworkers observed suppression of chaos in kicked spin and the kicked rotator systems [1,2,4]. Using a one-dimensional problem with a Duffing potential without any external perturbation, so that both classical and quantum behaviors are regular, Pattanayak and Schieve [9] demonstrated that the squeezed state behavior is chaotic, and concluded that the quantum fluctuations induce chaos. The effect of enhancement was also confirmed in a kicked double well model [6]. We shall see later that the KHO model provides a prototype for studying these two effects. The enhancement and suppression can be observed by changing the strength of the kicks.

The Hamiltonian of the quantum KHO model can be written as [18]

$$\hat{H} = \frac{\hat{p}^2}{2} + \frac{\omega_0^2}{2}\hat{q}^2 + V(\hat{q})\,\delta_T, \tag{22}$$

where

$$\delta_T = \sum_{n=-\infty}^{\infty}\delta(t - nT). \tag{23}$$

Using the squeezed state as a trial wave function of Hamiltonian (22), one can readily obtain

$$H=H_o+H_f+H_p, \tag{24}$$

where

$$H_o=\frac{p^2}{2}+\frac{\omega_0^2 q^2}{2} \tag{25}$$

is the Hamiltonian of the harmonic oscillator;

$$H_f=\frac{\Delta p^2}{2}+\frac{\omega_0^2 \Delta q^2}{2} \tag{26}$$

denotes the contribution from quantum fluctuations, and

$$H_p=\exp\left[\frac{\Delta q^2}{2}\left(\frac{\partial}{\partial q}\right)^2\right]V(q)\,\delta_T \tag{27}$$

denotes the contribution from the external perturbative potential. The external potential can be even or odd. Without loss of generality, we denote it as

$$V(q)=K\Theta(q), \qquad \Theta(q)=\begin{cases}\sin(k_0 q) & \text{for odd}\\ \cos(k_0 q) & \text{for even.}\end{cases} \tag{28}$$

From Eqs. (15) and (16), we have

$$\dot{q}=p, \qquad \dot{p}=-\omega_0^2 q-K_{\text{eff}}\Theta'(q)\,\delta_T, \qquad \dot{G}=4\Pi G, \qquad \dot{\Pi}=\frac{1}{8G^2}-2\Pi^2-\frac{\omega_0^2}{2}+\frac{k_0^2}{2}K_{\text{eff}}\Theta(q)\,\delta_T, \tag{29}$$

where

$$K_{\text{eff}}=K\,\exp\left(-\frac{\hbar k_0^2 G}{2}\right) \tag{30}$$

is called the effective potential, whose physical meaning will be discussed below. Θ' is the first derivative of Θ with respect to q. It is clear to see from Eq. (29) that, in the time interval $nT<t<(n+1)T$, the harmonic oscillator takes the free motion governed by

$$\dot{q}=p, \qquad \dot{p}=-\omega_0^2 q, \qquad \dot{G}=4\Pi G, \qquad \dot{\Pi}=\frac{1}{8G^2}-2\Pi^2-\frac{\omega_0^2}{2}, \tag{31}$$

while, at the time $t=(n+1)T$, it is kicked by the external potential. Therefore, before and after the kick the momentum and its fluctuation undergo jumps:

$$p_{n+1}(T^+)=p_n(T^-)-Ke^{-[\hbar G_n(T^-)]/2}\Theta'[q_n(T^-)], \qquad \Pi_{n+1}(T^+)=\Pi_n(T^-)+\frac{k_0^2}{2}Ke^{-[\hbar G_n(T^-)]/2}\Theta[q_n(T^-)]. \tag{32}$$

Equations (31) and (32) are coupled differential equations. From these equations, we can readily see that the squeezed state dynamics differs from the classical one in two ways. (1) There are two additional dimensions for the squeezed state motion, namely, the particle moves in a four-dimensional extended phase space. (2) The classical quantities (q,p) are coupled with the quantum fluctuations, which make the semiquantal motion complicated. On the one hand, because of these two additional dimensions in phase space, we expect that invariant curves in classical phase space would not be able to prevent the trajectory from penetrating or crossing them semiquantally. On the other hand, since the quantum fluctuations are always positive, they equal zero only in the limiting case of $\hbar=0$; the effective potential strength K_{eff} is always less than K. The reduction of the effective potential acting on the wave packet leads to the suppression of chaos. These two mechanisms coexist in the semiquantal system. They compete with each other and determine the dynamical behavior of the underlying system. Therefore, we expect that quantum fluctuations may not only enhance chaos but also suppress classical diffusion as well. This argument will be nicely illustrated in the following.

In this section we restrict our calculations on the potential

$$V(q)=-K\,\sin(q). \tag{33}$$

However, we should point out that the main conclusions given in this section do not depend either on the parity of the potential or the sign of K.

A. Enhancement of chaos

In solving Eqs. (31) and (32), we used the seventh and eighth order Runge-Kutta formula with adaptive stepsize control. The permissible error is fixed at 10^{-12}. In Fig. 1(a), we plot the classical phase space $(q_{\text{cl}},p_{\text{cl}})$ for a trajectory starting from (0,0) and evolving 10^4 kicks. The parameters $K=0.8$ and $\sigma=1/\pi$, where

$$\sigma=\frac{\omega_0}{\omega_T} \tag{34}$$

is the ratio between the angular frequency of the kicks ω_T ($\omega_T=2\pi/T$, T is the period of the kicks) and the angular frequency of the harmonic oscillator ω. In our calculations, we put $\omega_0=1$. It is obvious that, in classical phase space, regular (stable islands) and chaotic regions coexist. Figure 1(b) shows the time evolution of expectation values (q,p) of the wave packet for 10^4 kicks. The wave packet starts from $(q_0,p_0,G_0,\Pi_0)=(0,0,0.5,0)$, with $\hbar=0.1$. The selection of initial conditions $G_0=0.5$ and $\Pi_0=0$ follows the minimum uncertainty and least quantum effect conditions given in Sec.

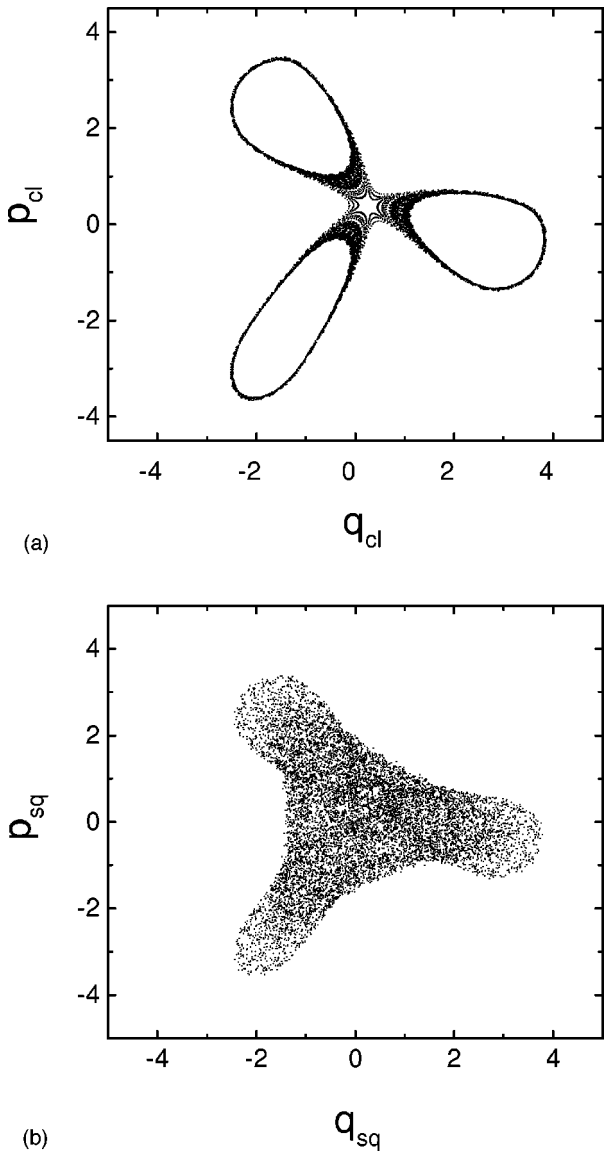

FIG. 1. Classical phase space (a) and time evolution of expectation values (p,q) of a wave packet (b) at $K=0.8$ for an irrational frequency ratio $\sigma=1/\pi$. One classical trajectory starts from (0,0). The wave packet starts from a point having an initial fluctuation parameter $(G_0,\Pi_0)=(0.5,0)$, and $\hbar=0.1$. The initial wave packet is a coherent state, i.e., it has same width in both p and q directions.

II. Therefore, the initial wave packet has the same width in both q and p directions, that is, it is a coherent state. If there are no kicks, the wave packet starting from this point will evolve exactly along the classical particle's trajectories forever. The fluctuations both in momentum and coordinate keep constant, and are independent of time. In this case, the squeezed state dynamics exactly describes the classical one. Now, if we switch on the kick, the situation becomes quite different. As is shown in Fig. 1(a), the initial point just lies in stochastic sea; thus it is evident that in the classical case the trajectory will never enter into stable islands due to the existence of invariant curves. However, as we predicted, the invariant curves are not able to prevent the trajectory from crossing it via other dimensions semiquantally. This is demonstrated by Fig. 1(b), where all stable islands in the classical phase space are ''visited'' by the semiquantal trajectory.

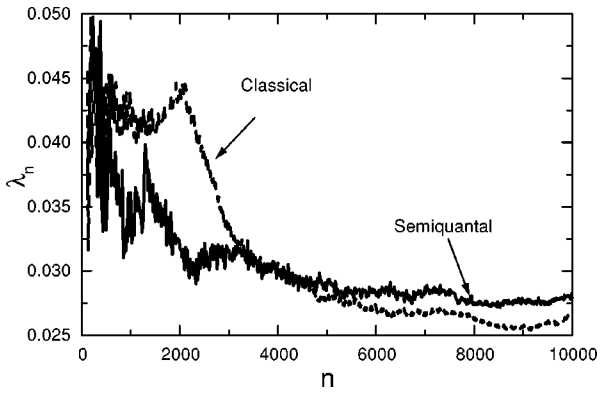

FIG. 2. Time (in units of the kick) behavior of λ_n for the trajectory shown in Fig. 1. The increment of λ_n after a certain time in the semiquantal case indicates the enhancement of chaos.

As a quantitative verification, we have numerically calculated the maximal Lyapunov exponent

$$\lambda=\lim_{n\to\infty}\lambda_n \tag{35}$$

for the trajectories in both cases. The time behavior of λ_n is shown in Fig. 2. It demonstrates the coexistence of enhancement and suppression. At the initial stage the enhancement mechanism is dominant. However, after a certain time, λ_n of the squeezed state becomes larger than its classical counterpart, which means that the enhancement mechanism becomes dominant, and consequently leads to enhancement of chaos. Furthermore, the chaotic motion in the extended phase space is characterized by two positive Lyapunov exponents in four-dimensional phase space $(q,p,\hbar G,\Pi)$, which could be verified readily.

B. Suppression of chaos

We would like go to another limit, namely, very large perturbation, to investigate the suppression of chaos. Classically, when K increases, the motion becomes more and more chaotic. For a sufficient large K such as $K=6$, the classical motion is completely chaotic, as shown in Fig. 3(a), where $\sigma=1/\pi$. Like Fig. 1, Fig. 3 is for a trajectory starting from the origin and evolving 10^4 kicks. The classical chaotic and diffusive process is easily seen from the evolution of this phase plot. To demonstrate the suppression of chaos (or diffusion process), we start a wave packet from (0,0,0.5,0) in the four-dimensional (4D) squeezed state phase space. The evolution is shown in Fig. 3(b). Comparing Figs. 3(a) and 3(b), it is obvious that, in the classical case, the phase space is chaotic and diffusive, whereas in the semiquantal case the diffusion process is largely slowed down and suppressed. There are invariant-curve-like structures that appear in the semiquantal phase space. These structures seem to form a barrier for diffusion and thus suppress chaos. The suppression of chaos is quantitatively demonstrated by the large decrease of λ_n, as is shown in Fig. 4, where the suppression mechanism is most important.

To illustrate the suppression, we plot variation of $K_{\rm eff}$ with time (in units of kicks) in Fig. 5. This plot indeed demonstrates that the effective perturbation strength is much less than its classical counterpart for most of the time during the

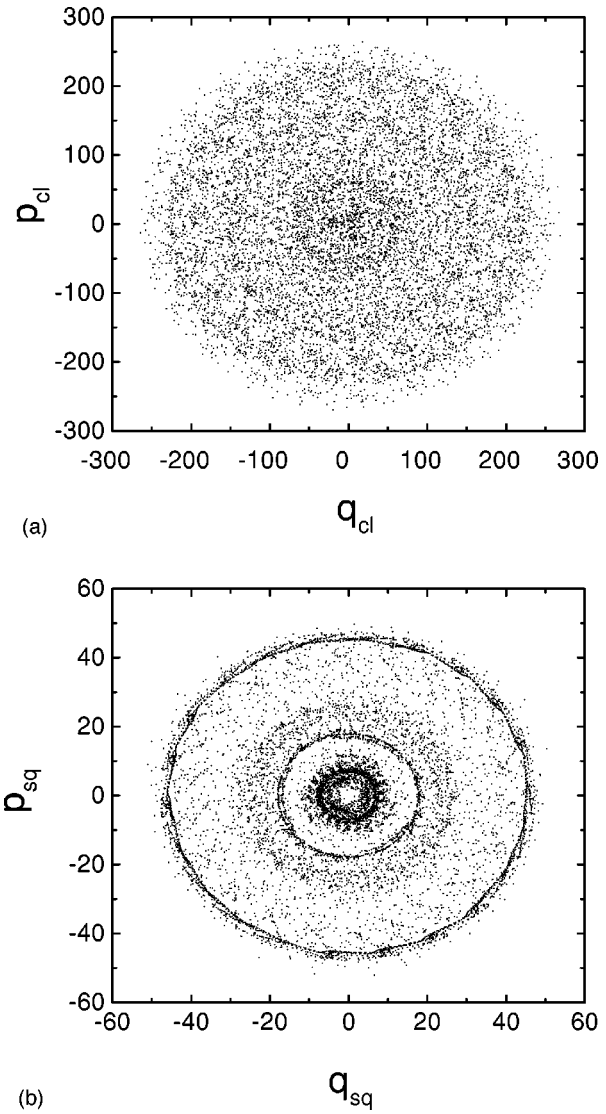

FIG. 3. Same as Fig. 1 but for $K=6$ with an irrational frequency ratio $\sigma=1/\pi$ for classical (a) and squeezed state (b) cases ($\hbar=1$). The semiquantal phase space shows an obvious suppression of the classical diffusion.

evolution. This is the reason for the suppression. In fact, the deduction of the effective potential acting on the wave packet has a clear physical picture. The width of a wave packet centered at (q,p) in coordinate space is $\Delta q=\sqrt{\hbar G}$, and the external potential has a wavelength of $2\pi/k_0$. Therefore, there are, in fact, $m(=\sqrt{\hbar G}k_0/2\pi)$ periods of external potential acting on the wave packet simultaneously. This is quite different from the classical model, where only one kick acts on a particle at one time. Since the external potential is negative in some places and positive in other places, the wider the wave packet, the larger the number of m, and therefore, the smaller the effective potential acting on the harmonic oscillator. However, if the wave packet Δq is so small that it is smaller than the period of the external potential, then the effective potential is large. As a matter of fact, the effective potential $K_{\rm eff}$ in Eq. (30) can be written as

$$K_{\rm eff}=K\ \exp\left(-\frac{m^2}{2\pi^2}\right). \tag{36}$$

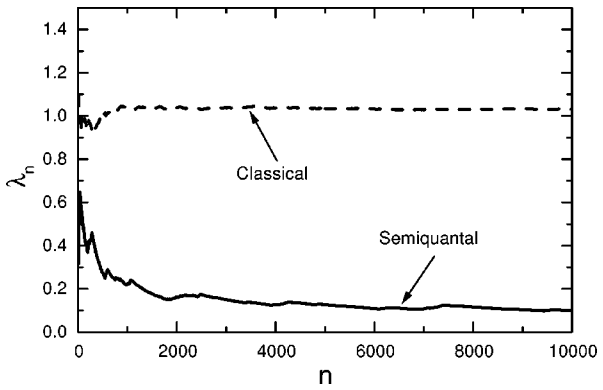

FIG. 4. Time behavior of λ_n for the trajectory shown in Fig. 3. The large decrement of λ_n in the semiquantal case demonstrates the strong suppression of classical diffusion.

As a significant evidence of the suppression, it is convenient to calculate energy diffusion with time n (in units of kicks) for an ensemble of trajectories. The diffusion is defined by $\langle E_n\rangle$ subtracts initial averaging energy $\langle E_0\rangle$, where $\langle\cdots\rangle$ means ensemble the average over many trajectories. In our calculations we have taken such an ensemble averaging over 10^4 initial points which are uniformly distributed inside a disk area centered at the origin of the phase space. For the classical one, $E_n=\frac{1}{2}(p_n^2+q_n^2)_{\rm cl}$, and for semiquantal dynamics, E_n is defined by

$$E_n=\frac{1}{2}\langle\Psi|\hat{p}_n^2+\omega_0^2\hat{q}_n^2|\Psi\rangle$$
$$=\frac{1}{2}(p_n^2+\omega_0^2q_n^2)+\frac{1}{2}\hbar\left(\frac{1}{4G_n}+4\Pi_n^2G_n+\omega_0^2G_n\right). \tag{37}$$

In Fig. 6, we show the energy diffusion of $K=6$ and $\sigma=1/\pi$ for classical and semiquantal cases. The suppression of classical diffusion is very obvious.

C. Transition from enhancement to suppression

We have seen so far that enhancement may happen at the small K regime, and suppression at the large K regime. Now we would like to discuss the transition from enhancement to suppression by changing the strength of the external poten-

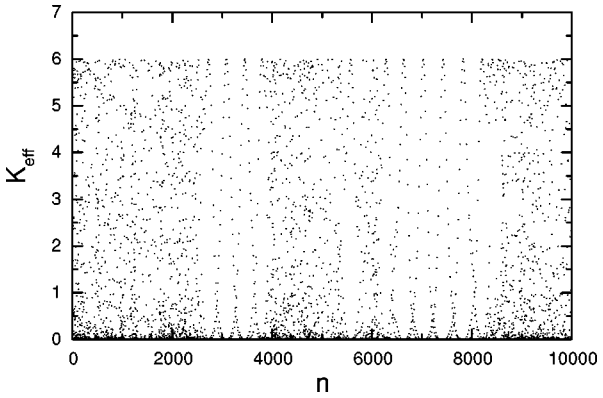

FIG. 5. Time evolution of the effective external potential $K_{\rm eff}$ for the orbit shown in Fig. 3.

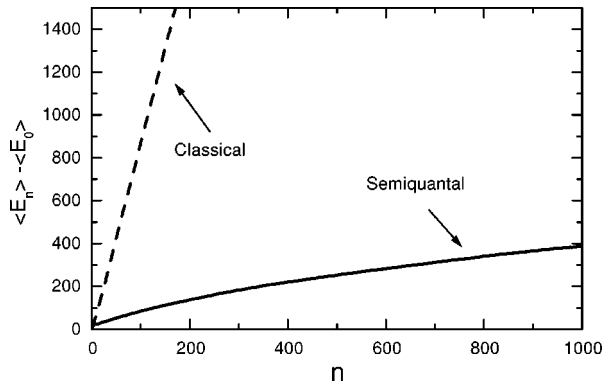

FIG. 6. Energy diffusion at $K=6$ for an irrational frequency ratio $\sigma=1/\pi$ for classical and semiquantal cases. The ensemble averaging is taken over 10^4 initial points which are uniformly distributed in an area of the disk centered at (0,0) with a radius of π in the phase space. The diffusion coefficient in the semiquantal case is obviously much smaller than that of the classical case, which indicates a strong suppression of classical chaos.

tial for fixed quantum fluctuations. Here we want to show that there exists a threshold value of K_c distinguishing enhancement from suppression.

To this end, we need to take an appropriate ensemble average over many trajectories in phase space. However, since the classical phase space of the KHO model is unbounded, it is impossible to do such an average over the whole phase space. This makes numerical works very difficult. After many numerical experiments, we find a compromise, namely, we take the average over a disk centered at origin with radius π. We spread 15×15 initial points uniformly distributed inside this area. In classical case, we calculate the Lyapunov exponent for each trajectory after 10^4 kicks, and plot the averaged value denoted as $\langle\lambda_{\mathrm{cl}}\rangle$ in Fig. 7. This averaged value is in analogy to the Kolmogorov entropy in a bounded system. However, strictly speaking, this quantity cannot be called Kolmogorov entropy. Nevertheless, this parameter captures more or less chaoticity of the underlying system. In the case of semiquantal dynamics, since we have 4D extended phase space, we always have two positive

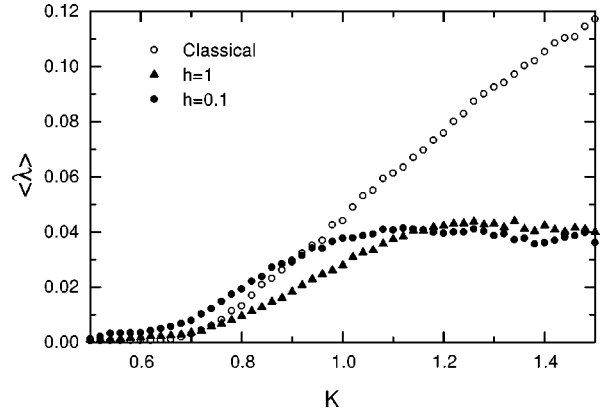

FIG. 7. Transition from enhancement to suppression. The averaged Lyanpunov exponent vs the external potential K for classical and semiquantal cases with $\hbar=0.1$ and 1. The average is taken over 15×15 points uniformly distributed inside a disk of radius π centerd at (0,0). Here $\sigma=1/\pi$.

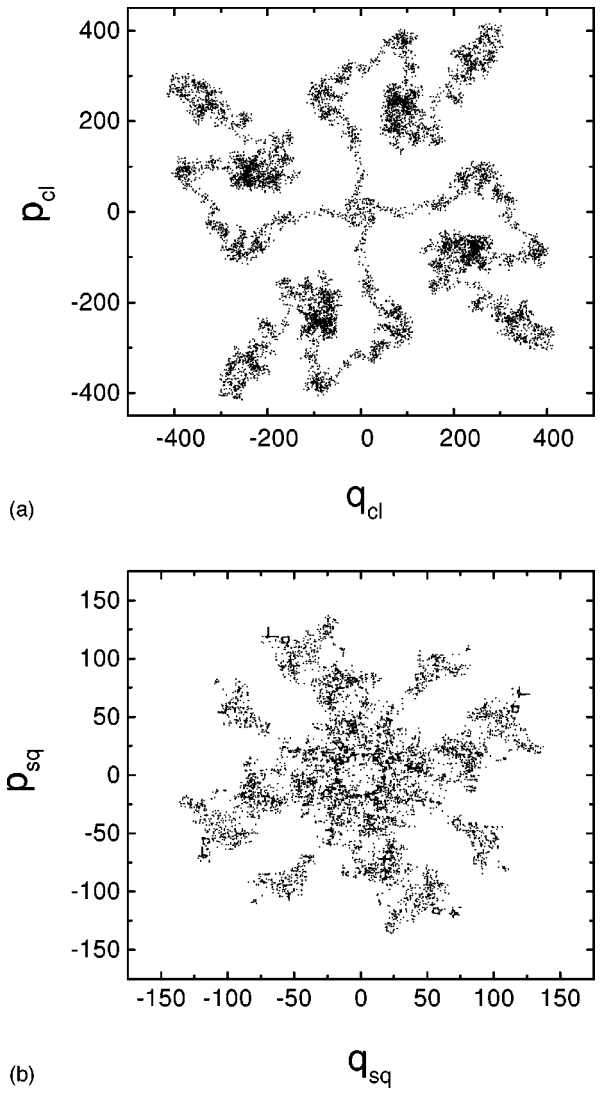

FIG. 8. Demonstration of suppression for a rational $\sigma=1/4$ frequency ratio and $K=6$. (a) Classical phase space. (b) Semiquantal $(q_{\mathrm{sq}},p_{\mathrm{sq}})$ with $\hbar=1$.

Lyapunov exponents. We add these two values, and denote the result as $\langle\lambda_{\mathrm{sq}}\rangle$. It is plotted in Fig. 7 in comparison with the classical result.

From Fig. 7 we can draw the following conclusions: (1) There exists a certain threshold value of K_c. Before this point, $\langle\lambda_{\mathrm{sq}}\rangle>\langle\lambda_{\mathrm{cl}}\rangle$, which means that the degree of chaos is enhanced; after this point, $\langle\lambda_{\mathrm{sq}}\rangle<\langle\lambda_{\mathrm{cl}}\rangle$, chaos is suppressed. This critical value K_c changes with $\hbar$. (2) At the region of $K\gg K_c$, $\langle\lambda_{\mathrm{sq}}\rangle$ fluctuates around a certain value. It does not change with K. (3) The enhancement and suppression depends largely on $\hbar$.

The results discussed in this section are restricted to an irrational frequency ratio. One might ask whether our conclusion also applies to the rational frequency ratio. It is well known that the KHO model is a degenerate system out of the KAM theorem. In classical phase space, there exists a slow diffusion along the stochastic web for any small value of perturbation. Our numerical results also show enhancement and suppression. We give one example of rational frequency ratios $\sigma=1/4$ and $K=6$ in Fig. 8 for suppression. The corresponding Lyapunov exponent is shown in Fig. 9.

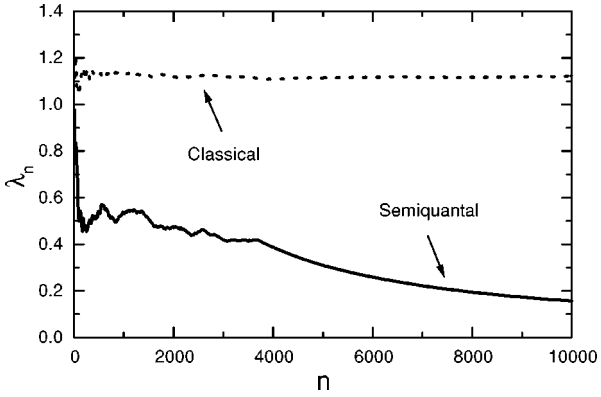

FIG. 9. The Lyapunov exponent for the trajectory shown in Fig. 8.

Finally, we would like to say a few words about the initial conditions and parity of the external potential. We have performed a wide range of numerical investigations, and found that the above discussed qualitative and quantitative conclusions are independent of the selection of the initial condition and the parity of the external potential. However, the selection of the initial condition must be physically meaningful, as we discussed in Sec. II.

Before concluding this section, we would like to discuss the connection of suppression to the dynamical localization. In fact, this is a challenge to the squeezed state approach for this subtle phenomenon. We argued that the dynamical localization observed in a kicked rotator is due to a suppression of the chaos discussed above. In fact, in the limiting case of $\omega_0=0$, the KHO model [Eq. (22)] is reduced to the kicked rotator model, in which chaotic diffusion is completely suppressed by the quantum fluctuations and results in dynamical localization, a well established fact observed numerically by Casati *et al.* [15] almost 20 years ago, and confirmed recently by experiment [17]. This was nicely illustrated by Zhang and Lee [4] with the squeezed state approach.

IV. DIFFUSION AND LOCALIZATION

In Sec. III we showed how quantum fluctuations enhance and suppress chaos. This fact will definitely affect diffusion behavior. For instance, in the limiting case, when the suppression becomes dominant, localization is expected to happen. In this section we shall give a detailed study of this. In particular, we concentrate on the large K regime. This is the most difficult region in pure quantum computation. As we shall see, the squeezed state approach not only provides an easy way to do numerical calculations but also makes it possible to do some analytical estimations.

The energy E_n of the kicked harmonic oscillator in the squeezed state approximation [Eq. (37)] can be written as two parts:

$$E_n=E_n^c+E_n^f. \tag{38}$$

E_n^c contains the first two terms in Eq. (37), which is due to the motion of the centroid of a wave packet. They mimic the effect of classical diffusion (ECD). E_n^f includes the last three terms in Eq. (37), and is attributed to the effects of quantum fluctuations (EQF). These two kinds of effects are the main ingredients of the diffusion process in the squeezed state dynamics.

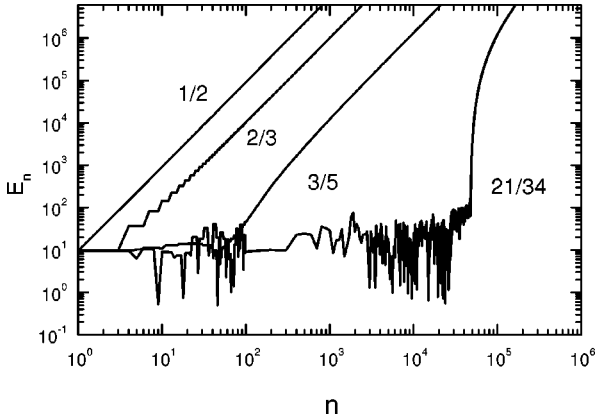

FIG. 10. Evolution of the energy with time (in units of kicks) for the case of an even potential with a rational frequency ratio. Numbers in the plot indicate the frequency ratio. The case of 1/1 coincides with that of 1/2. Note that the curves have slope 2 asymptotically, and a transient dynamical localization phenomenon shows up.

The ratio σ is an important quantity, as we shall see soon. We take σ, the golden mean value $\sigma_g=(\sqrt{5}-1)/2$, and its continued-fraction expansion r/s: $\frac{2}{3},\frac{3}{5},\frac{5}{8},\ldots$ as examples. r and s are generated by the Fibonacci sequence defined by $F_0=1$, $F_1=1$, and $F_n=F_{n-2}+F_{n-1}$ for $n>1$. Without loss of generality, in all calculations, we keep parameters $\hbar=1$, $K=6$, $k_0=1$, and $\omega_0=1$, and the initial point is chosen as (0,0,0.5,0), which corresponds to the ground state of unperturbed quantum harmonic oscillator.

A. Numerical results

Figures 10 and 11 and 12 and 13 show our numerical results of energy diffusion of

$$V(q)=\begin{cases}K & \cos(k_0q)\\ K & \sin(k_0q)\end{cases} \tag{39}$$

for even and odd parity, respectively. Now we discuss these two cases separately.

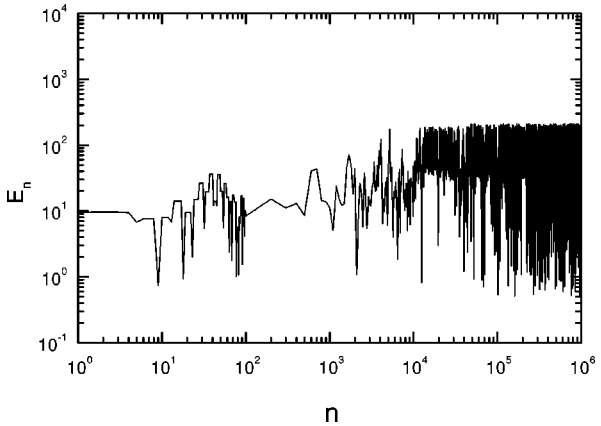

FIG. 11. Same as Fig. 10, but for an irrational frequency ratio $\sigma=(\sqrt{5}-1)/2$. The localization is obvious.

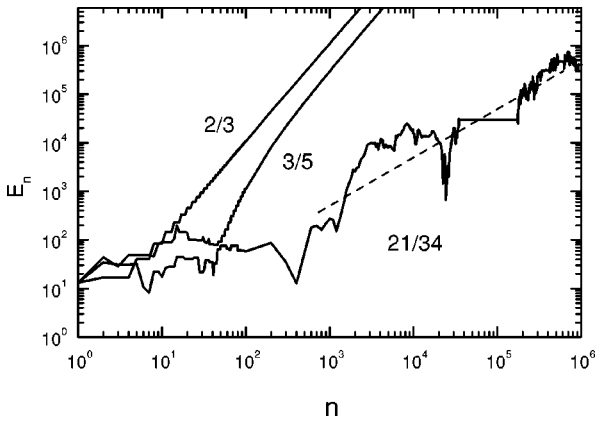

FIG. 12. Same as Fig. 10, but for the case of odd potential. The dashed line with slope 1 is drawn to guide the eye.

Even potential: In this case, for all rational frequencies, the energy will finally go quadratically with time, i.e., $E_n \sim n^2$. As shown in Fig. 10, the slope equals 2 asymptotically in the double logarithmic plot. However, for the case $\sigma = r/s$ with relatively larger r and s, the diffusion starts only after a certain time. Before this time the energy diffusion is localized. The transient time depends on the frequency ratios, and is approximately of the order of $(\sigma-\sigma_g)^{-1}$. We call this transient region a *transient dynamical localization* region.

For the irrational case, dynamical localization occurs, as clearly demonstrated in Fig. 11. This significant phenomenon has been observed and investigated in various quantum systems in past few years.

It is worth pointing out that for two trivial cases, i.e., $\sigma = \frac{1}{1}$ and $\frac{1}{2}$, our squeezed state results given here agree *completely* with the quantum analytical results of Ref. [20] which has been the only existing analytical results of the quantum diffusion of this model up to now. This demonstrates the usefulness of the squeezed state approach. Moreover, by using the squeezed state approach, we have also recovered the quantum results obtained numerically by Borgonovi and Rebuzzini [21]. For more details, see Sec. V.

Odd potential: In this case, quadratic law is observed only in the case of rational frequency ratios $\sigma = r/s$ with odd s. For other situations the energy diffuses linearly with time approximately; see Figs. 12 and 13.

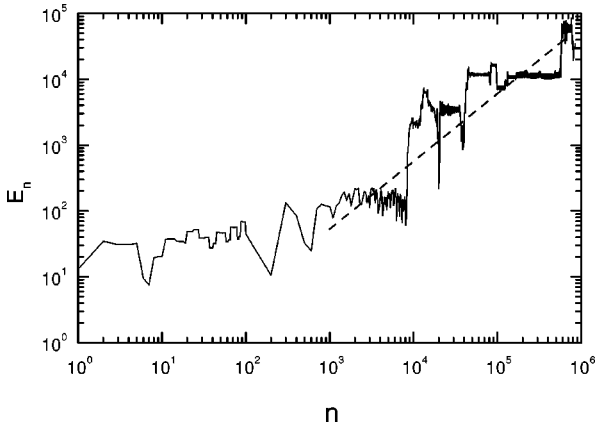

FIG. 13. Same as Fig. 11 but for the case of odd potential. The dashed line with slope 1 is drawn to guide the eye.

B. Analytical estimates

The above numerical results can be understood by analyzing evolution equations (29). In fact, we can analytically derive the energy diffusion by studying system (29). Starting from Eqs. (29), we find that when the external perturbation is absent, the two degrees of freedom (DOF's) (p,q) and (G,Π) are decoupled, and each undergoes free motion. In terms of action-angle variable, the Hamiltonian of the free motions can be expressed as Eq. (A5). From this formula, we have already seen that *both* free motions of the two DOF's are *degenerate*. It is this degeneracy which makes resonance between the two frequencies possible in phase space. Consequently, the squeezed state dynamical behavior of the kicked harmonic oscillator is quite different from that of the kicked rotator [4]. That is, the motions of the centroid and the fluctuations of the wave packet behave like an oscillator with fixed frequencies ω_0 and $2\omega_0$, respectively.

However, when kicks are added, the two degree of freedom becomes coupled, and energy may start to diffuse. It is convenient to express the evolution of system in terms of action-angle variables. From Eqs. (A4) and (A5) one can readily obtain four-dimensional maps

$$
\begin{aligned}
I_{n+1} &= I_n - K_{\mathrm{eff}}\Theta'(k_0\sqrt{2I_n/\omega_0}\,\sin\,\phi_n)k_0\sqrt{2I_n/\omega_0}\,\cos\,\phi_n,\\
\phi_{n+1} &= \phi_n + \omega_0 T\\
&\quad + K_{\mathrm{eff}}\Theta'(k_0\sqrt{2I_n/\omega_0}\,\sin\,\phi_n)k_0/\sqrt{2I_n\omega_0}\,\sin\,\phi_n,
\end{aligned}
\tag{40}
$$

$$
\begin{aligned}
J_{n+1} &= J_n + K_{\mathrm{eff}}\frac{\hbar}{4}k_0^2\sqrt{(4J_n+1)^2-1}\\
&\quad \times \sin\,\theta_n\Theta(k_0\sqrt{2I_n/\omega_0}\,\sin\,\phi_n),\\
\theta_{n+1} &= \theta_n + 2\omega_0 T - K_{\mathrm{eff}}k^2\hbar\left(1-\frac{4J_n+1}{\sqrt{(4J_n+1)^2-1}}\cos\,\theta_n\right)\\
&\quad \times\Theta(k_0\sqrt{2I_n/\omega_0}\,\sin\,\phi_n).
\end{aligned}
$$

With this 4D map, we are able to perform an analytical estimate of the energy diffusion. We shall treat it at two different limiting cases.

Classical diffusion effect ($\hbar = 0$)

In the classical limit case, $\hbar = 0$ and $E_n^f = 0$, and the effect of classical diffusion becomes dominant. Therefore, the change of energy during one kick is

$$
\begin{aligned}
\Delta E_n^c &= k_0 K\Theta'(k_0 q_n)(p_n\,\cos\omega_0 T - q_n\omega_0\,\sin\,\omega_0 T)\\
&\quad + \tfrac{1}{2}k_0^2K^2\Theta'^2(k_0 q_n).
\end{aligned}
\tag{41}
$$

For $K \gg 1$, the orbit can be supposed to be approximately ergodic. After ensemble averaging over variables p and q, the first two terms vanish approximately; thus we obtain linear energy diffusion

$$
E_n^c \sim \langle \Delta E_n^c\rangle n \approx \tfrac{1}{4}k_0^2K^2 n. \tag{42}
$$

Note that the average of the first two terms of ΔE_n^c, though is much smaller than the last term for large K, is nevertheless

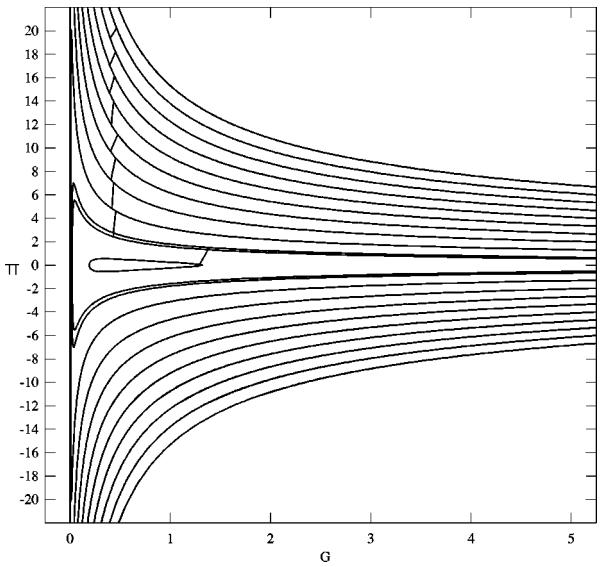

FIG. 14. Evolution (G,Π) plot for $K=6$ and $\sigma=2/3$.

not exactly zero. This results in some oscillations of E_n around the linearity (see Figs. 12 and 13).

Effect of quantum fluctuations

For the second limit case, suppose a wave packet starts from $(q,p,G,\Pi)=(0,0,0.5,0)$ with an even potential, and the center of the wave packet keeps fixed; thus $E_n^c \equiv 0$. The energy diffusion is caused purely by the effects of the quantum fluctuations. In this case we shall analyze the diffusion process for two different frequency ratios, i.e., rational and irrational. For the rational frequency ratio, let us take the simple case of $\sigma=\frac{2}{3}$ as an example. During a time of $3T$, there are three kicks acting on the harmonic oscillator. Since the frequency of fluctuation is $2\omega_0$, (G,Π) evolves four periods. Note that the effective amplitude of a kick acting on the wave packet is K_{eff} rather than K. Among these three kicks, *only* that one at a relative small G affect the free motion of the oscillator significantly. We call this kick the *effective* kick; the effects from other two kicks can be neglected due to a very large G, and consequently a very small K_{eff}. At the time when the next *effective* kick is in action, G is approximately the same because of the resonance; see Fig. 14. Therefore, the increment of Π is almost constant, which means that $\Pi_{3n} \approx n$. Thus, from Eq. (37), we obtain

$$E_n \approx n^2, \tag{43}$$

which gives rise to the quadratic law observed in Figs. 10 and 12.

If σ is an irrational number, a very interesting thing will happen. From Eq. (A3) we know that the angular variable when a kick is added is

$$\theta_n = 2\pi n\sigma + \theta_0 (mod 2\pi). \tag{44}$$

This is nothing but a pseudorandom number generator, indicating that the jump of Π may happen in upper $(\Pi>0)$ and lower $(\Pi<0)$ parts with the same probability, and thus the increment of energy in the upper part will be canceled out by the decrease in the lower part. This leads to the localization phenomenon observed in Fig. 11. This localization mechanism, resorting to a pseudorandom number generator, reminds us what happens in the kicked rotator, where the localization is related to Anderson's localization for a quantum particle propagating in a one-dimensional lattice in the presence of a static-random potential [16]. Our results imply that it might also be possible to construct a connection between the kicked harmonic oscillator and Anderson's problem in the framework of the squeezed state approximation. The mechanism discussed can also explain the transient dynamical localization that occurs in the case of the rational frequency ratio, as shown in Fig. 10. Since, during the time $t \leqslant (\sigma-\sigma_g)^{-1}$, a rational number behaves just like a pseudoirrational number, a transient localization phenomenon occurs.

General case

As to the general case of system (29), both the ECD and EQF may coexist. To illustrate this, we consider the case of $\sigma=r/s$, where r and s are coprimed integers. Suppose s is odd. As we have explained above, between two *effective* kicks, (q,p) and (G,Π) evolve freely. Thus the angle variables of (q,p) at the two successive *effective* kicks are ϕ and $\phi+2\pi r$, respectively, and that of (G,Π) are θ and $\theta+4\pi r$. From Eqs. (A5) and (29), we find that, in this case, the increment of Δp and $\Delta\Pi$ have the same sign, which means that both the ECD and EQF are excited, which is independent of the potential parity. Because the diffusion due to the EQF is $\sim t^2$, which is much faster than that of the ECD $(\sim t)$, thus asymptotically t^2 diffusion shows up, as shown in Fig. 12. However, if s is even, there is one additional *effective* kick between the above mentioned two, namely, the $s/2$th kick, at which the angle variable of (G,Π) is $\theta+2\pi r$, while that of (q,p) is $\phi+\pi r$. Thus, for the even potential case, the changes of Π due to the two consecutive *effective* kicks have the same sign, which implies that the EQF is excited and t^2 diffusion will show up. For the odd potential case, the changes of Π due to the two consecutive *effective* kicks have opposite sign, the EQF is thus suppressed, and we obtain the linear diffusion seen in Fig. 13.

For the irrational σ case, the EQF is suppressed and the ECD becomes dominant. If (p,q) happens to be a fixed point in the (p,q) plane, as is the case of Fig. 11, localization occurs. This is the reason for the different diffusion behaviors of irrational σ in Figs. 11 and 13 for even and odd external potentials, respectively. Please note that $(p,q)=(0,0)$ are the expectation values of all the eigenstates of the harmonic oscillator; thus the localization we observed in Fig. 11 is not restricted to the case of the ground state, as we discussed up to now, but is very general.

C. Transition from localization to diffusion

The results discussed above focused on diffusion at very large perturbation; in this case the underlying classical system is completely chaotic. As a further example we would like to demonstrate a very interesting and important phenomenon in quantum mechanics, i.e., the *tunneling effect*. We start a wave packet from point (0,7.5) in the classical phase space (q,p). Here we have $\sigma=\frac{1}{5}$ and $V(q)=K\cos q$ with $K=0.5$. The wave packet has parameters $G_0=\frac{1}{2}$ and Π_0

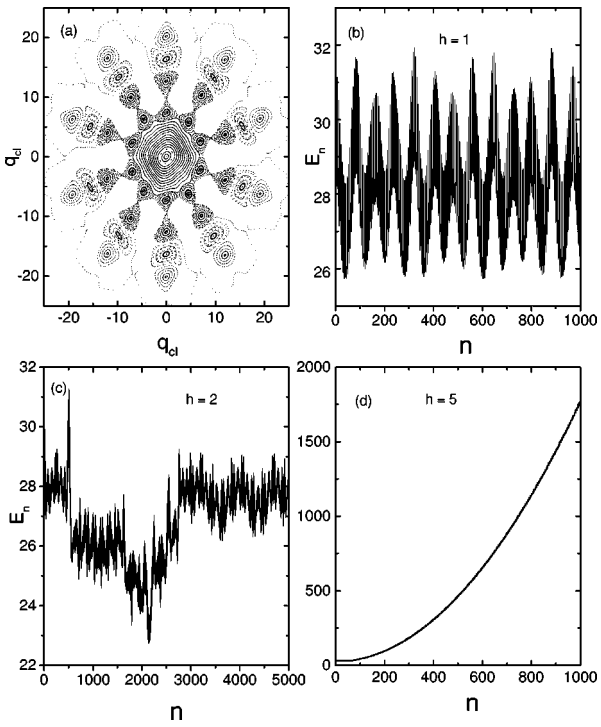

FIG. 15. Transition from localization to delocalization of a wave packet driving by the quantum fluctuations. The wave packet starting from a stable island $(q_0,p_0)=(0,7.5)$. $\sigma=1/5$, $\omega_0=1$, and $K=0.5$. (a) Classical phase space. (b)–(d) Semiquantal energy diffusion. (b) $\hbar=1$. (c) $\hbar=2$. (d) $\hbar=5$.

$=0$ according to the minimal uncertainty principle. It is a Gaussian wave packet. The classical phase space is shown in Fig. 15(a). We see that the starting point lies inside a stable island. Classically, a trajectory that starts from this point will never be able to escape. However, in the quantum case, the situation becomes very different. We expect that if the width of the wave packet is much smaller than the size of this stable island, the wave packet will be confined by this stable island, and thus lead to localization. However, if the wave packet becomes wider than the size of the stable island, it will spread out. Here we demonstrate this quantum phenomenon by the squeezed state approach. In Figs. 15(b)–15(d), we plot the energy evolution for different Planck constant $\hbar$, which corresponds to different widths of the initial wave packet. At $\hbar=1$ and 2, we observed a localization phenomenon as in other quantum systems. The energy oscillates around a certain value. When we increase $\hbar$ further to $\hbar=5$ a transition from localization to delocalization occurs, which is shown in Fig. 15(d).

V. COMPARISON WITH QUANTUM RESULTS

To give the reader a clear picture about the accuracy of the squeezed state approach, we would like to compare our results with those obtained from pure quantum computation. However, as mentioned above, since diffusion occurs in the whole unbounded phase space and cannot be reduced to motion on a cylinder like the case of a kicked rotator, a pure quantum (numerical) investigation is very difficult, in particular, in the large K regime. Nevertheless, with a large amount of CPU time, one would be able to obtain some

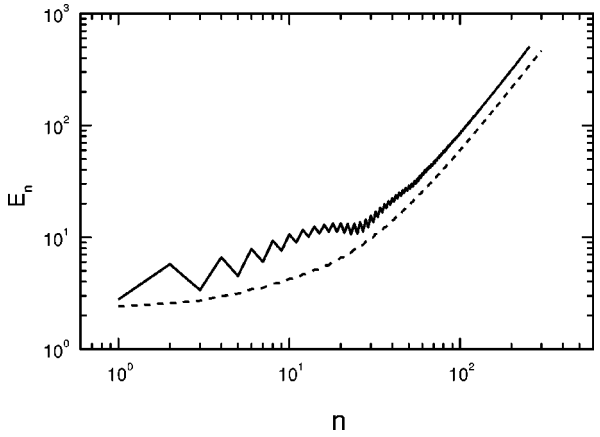

FIG. 16. Comparison of semiquantal (dashed line) and quantum (solid line) diffusion for $\sigma=\frac{1}{4}$, $\omega_0=2/\pi$, $\omega_1=8\pi$, $K=0.5$, and $\hbar=1$. The trajectory starts from $(q_0,p_0)=(3.15,0)$. The semiquantal trajectory has the same (q_0,p_0) and $(G_0,\Pi_0)=(1/2\omega_0,0)$. Please compare it with Fig. 1 in Ref. [21].

results in the small K regime for short time evolution. This is why there are only limited available quantum results in this regime. We will compare them with our squeezed state results here.

First, let us look at the results obtained in Ref. [20], already shown in Fig. 10. As for the case of 1/1 and 1/2, our squeezed state results agree completely with the quantum one of Ref. [20]. In this case both squeezed state and pure quantal analyses predict t^2 growth of the energy. We should mention that it was conjectured in Ref. [20] that, for the general case of $1/q$, the energy growth should be less than t^2. From our squeezed state analysis we concluded that there are only three different diffusions: t^2, t and localization. Therefore, our squeezed state analysis also agrees with Ref. [20]'s prediction.

Now we turn to the results obtained by Borgonovi and Rebuzzini [21]. Since the time unit given in their pictures is not clear, we are not able to make any quantitative comparison with our squeezed state results. Therefore, we performed quantum calculations by using our own program (see Appendix B). All the system parameters are kept the same as that used by Borgonovi and Rebuzzini. The results are given in Figs. 16 and 17. These pictures correspond to different diffusion behaviors. In Fig. 16, a t^2 diffusion is obtained (t is in units of kicks); the squeezed state approach also gives rise to a t^2 diffusive behavior, although there is a difference in prefactor. In Fig. 17, both the quantum and squeezed state results show localization around approximately the same energy. Please compare these two pictures with Figs. 1 and 8 of Borgonovi and Rebuzzini [21], respectively.

Our quantum computation technique (Appendix B) is different from that used in Ref. [20]. For a self-consistent test, we have used the same parameter as that of Fig. 2 in Ref. [20], and computed the energy diffusion with our method. We found that our results agree those of Ref. [20] in every detail.

As already emphasized, because of the unbounded phase space, the quantum computation is very time consuming, even for small perturbation. For instance, about ten days CPU time (IBM RISC System/6000 42T, with 192 Mbyte

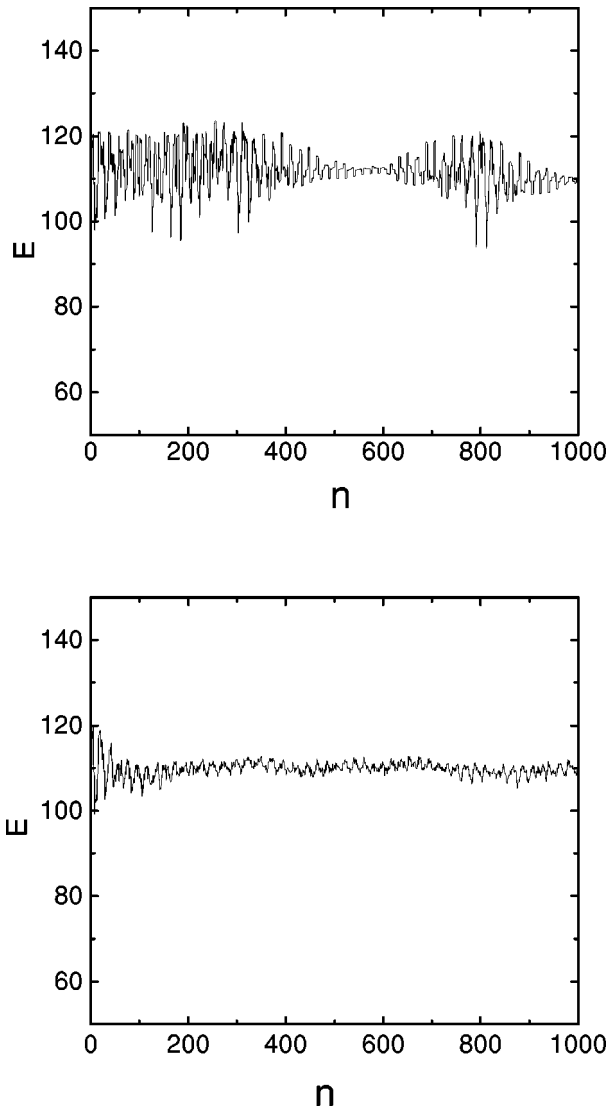

FIG. 17. Comparison of semiquantal (top) and quantum (bottom) diffusion for $\sigma=(\sqrt{5}-1)/2$, $\omega_0=1$, $K=1$, and $\hbar=1$. The trajectory starts from $(q_0,p_0)=(15,0)$. The semiquantal trajectory has the same (q_0,p_0) and $(G_0,\Pi_0)=(1/2\omega_0,0)$. Please compare it with Fig. 8 in Ref. [21].

RAM) has been spent for Fig. 16, and 20 days CPU time for Fig. 17.

VI. CONCLUSIONS AND DISCUSSIONS

Applying the squeezed state approach to the kicked quantum harmonic oscillator, we illustrate how the quantum fluctuations affect the classical dynamics. We have shown that chaoticity can be enhanced as well as suppressed by the quantum fluctuations. A transition from enhancement to suppression is observed when we change the strength of the kicks.

Moreover, with this squeezed state approach, we are able to investigate the energy diffusion. Three different energy diffusions have been observed for the kicked quantum harmonic oscillator, namely, localization, linear diffusion, and quadratic diffusion. The localization is due to strong suppression.

Though it is a kind of approximation, the squeezed state can mimic many true quantum behaviors such as those demonstrated in this paper. Moreover, there are examples showing that the squeezed state approach gives rise to better results than the semiclassical method. However, under which condition or how far the squeezed state approach can go beyond the semiclassical method is still an open problem that deserves further numerical as well as theoretical study.

Finally, we would like to remark on the quantization of a quantum system whose classical counterpart is chaotic. As is well known, this is a tough problem which has attracted tremendous attention in last two decades. Among many others, Gutzwiller's trace formula might be the most plausible one [27]. However, this approach encountered difficulty of divergence, although many important contributions have been made to overcome this difficulty. We believe that the squeezed state approach might be an alternative way that can contribute to this. Recent successful application of this method by Pattanayak and Schieve [11] to calculate eigenenergies of a chaotic system sheds light on this direction.

ACKNOWLEDGMENTS

We would like to thank Dr. L.-H Tang and Dr. F. Borgonovi for many stimulating discussions. The work was supported in part by grants from the Hong Kong Research Grants Council (RGC) and the Hong Kong Baptist University Faculty Research Grant (FRG).

APPENDIX A: QUANTIZATION OF THE HARMONIC OSCILLATOR BY THE SQUEEZED STATE APPROACH

In this appendix, we would like to demonstrate how the squeezed state works when applied to a simple quantum system, a harmonic oscillator, which is the KHO system with a zero external potential. The harmonic oscillator is a simple but very important model in quantum mechanics. It is an integrable system, and its eigenenergies as well as eigenfunctions can be obtained analytically. Therefore, this model is very suitable for testing approximate methods such as the WKB method and others.

It is well known that the WKB approximation can give us exact eigenenergies for this integrable system. However, it cannot yield exact eigenfunctions, in particular, for the low-lying eigenstates. It gives only the envelope of the wave function in the semiclassical limit $\hbar\to 0$. In this appendix, we shall demonstrate that when applying the squeezed state approach to the harmonic oscillator model, one can obtain the energy levels precisely as well as the eigenfunctions.

The harmonic oscillator has the Hamiltonian operator

$$\hat{H}=\frac{\hat{p}^2}{2}+\frac{\omega_0^2\hat{q}^2}{2}. \tag{A1}$$

Applying the squeezed state approach to this system, one can easily obtain

$$H=\frac{p^2}{2}+\frac{\omega_0^2 q^2}{2}+\frac{\hbar}{2}\left(\frac{1}{4G}+4\Pi^2 G+\omega_0^2 G\right). \tag{A2}$$

This Hamiltonian can be expressed in terms of action-angle variables

$$H=\omega_o I+2\omega_0(J+\hbar\tfrac{1}{4}), \tag{A3}$$

where

$$I=\frac{1}{2\pi}\oint p\ dq, \quad J=\frac{1}{2\pi}\oint \Pi d(\hbar G). \tag{A4}$$

The transformations between (q,p), (G,Π) and (I,ϕ), (J,θ) have the following forms:

$$q=\sqrt{2I/\omega_o}\ \sin\ \phi,$$

$$p=\sqrt{2I\omega_o}\ \cos\ \phi, \tag{A5}$$

$$G=\frac{1}{\omega_0}\left[\left(2J+\frac{1}{2}\right)-\sqrt{2J(2J+1)}\ \cos\ \theta\right],$$

$$\Pi=\frac{\frac{\omega_0}{2}\sqrt{2J(2J+1)}\ \sin\ \theta}{(2J+\frac{1}{2})-\sqrt{2J(2J+1)}\ \cos\ \theta}.$$

From Eq. (A5) one can see that the motion of *both* degrees of freedom are *degenerate*, namely, $\partial H_o/\partial I$ is independent of I and $\partial H_f/\partial J$ independent of J. Furthermore, (G,Π) are decoupled from (q,p). Thus the centroid of the wave packet goes exactly along the classical trajectory. While the fluctuations in momentum and position are time independent, i.e., the width of the wave packet stays constant. From the minimal uncertainty principle for the initial condition mentioned in Sec. II, we have $G=1/2\omega_0$ and $\Pi=0$. Therefore, the wave packet along the periodic orbit always keeps its form as a coherent state.

The time evolution of both (q,p) and (G,Π) are periodic with period $T_0(=2\pi/\omega_0)$ and $T_0/2$, respectively. So we can apply the EBK quantization to the extended phase space,

$$I=n\hbar, \quad J=m\hbar, \quad n,m=0,1,2,\ldots, \tag{A6}$$

Substituting I and J into Eq. (A3) and keeping in mind that $G=1/2\omega_0$ and $\Pi=0$, and thus $m=0$, we obtain the squeezed state eigenenergy,

$$E_n=\hbar\omega_0(n+\tfrac{1}{2}). \tag{A7}$$

This is exactly the eigenenergy of the harmonic oscillator. Here the zero point energy $\frac{1}{2}\hbar\omega_0$ comes into the formula in a very natural and straightforward way. This is quite different from the WKB method. In the WKB method, $\frac{1}{2}\hbar\omega_0$ comes from the Maslov phase correction which is necessary because of the singularity of the wave function. In the squeezed state approach, since we do not have any singularities, the Maslov-Morse correction is incorporated by the extended variables G and Π. Furthermore, the energy of the system is in the form of the expectation value of the underlying Hamiltonian operator, whereas in the usual WKB method, the energy is taken to be the classical form, i.e., $E=H_{\rm cl}$. This is one of the reasons that people call this approach the *semiquantum approach.*

Let us now construct the eigenfunction by the squeezed state approach. We see that when the trial wave function $|\Psi(t)\rangle$ is transformed to

$$|\tilde{\Psi}(t)\rangle=\exp\left(\frac{i\lambda(t)}{\hbar}\right)|\Psi(t)\rangle, \tag{A8}$$

the derived variational equations of motion remain invariant. Substituting $|\tilde{\Psi}(t)\rangle$ into the Schrödinger equation, we can obtain the equation determining $\lambda(t)$,

$$\lambda(t)=\int_0^t dt'\langle\Psi(t')|ih\frac{\partial}{\partial t'}-\hat{H}|\Psi(t')\rangle=\lambda_G+\lambda_D. \tag{A9}$$

The second part of the integral corresponds to the dynamical phase. We denote it λ_D. The first term is the geometrical phase noted as λ_G, which is

$$\lambda_G=\tfrac{1}{2}\int_0^t(p\dot{q}-q\dot{p})dt+\hbar\int_0^t\dot{\Pi}G\ dt. \tag{A10}$$

Since the motions of (p,q) and (G,Π) are periodic, this geometrical phase is the Aharanov-Anandan form of Berry's phase. During the evolution, each point along the periodic orbit acquires a phase factor. However, the dynamical phase does not change during the evolution; only the geometrical phase matters. So the eigenfunction is a weighted sum over points of the commensurate periodic orbit [10]. The weight factor at each point is an appropriate geometrical phase. Furthermore, as mentioned above, according to the requirement of the initial condition, the initial wave packet is a coherent wave packet, and it does not change its form when cycling along the periodic orbit. Substituting expressions for p and q in Eq. (A5) into Eq. (A10), and keeping in mind that $\Pi=0$, we can easily evaluate the integral and obtain the geometrical phase at time t, which is

$$\lambda_G(t)=n\hbar\phi, \tag{A11}$$

where $\phi=\pi/2-\eta$. Thus the eigenfunction for the bound state having the eigenenergy E_n in Eq. (A7) is

$$c\int_0^{2\pi}e^{i(\lambda_G/\hbar)}|\alpha\rangle d\phi=C\int_0^{2\pi}e^{-in\eta}|\alpha\rangle d\eta, \tag{A12}$$

where $|\alpha\rangle$ is the coherent state, ϕ is the angle in the $(\omega_0 q,p)$ plane, and C is the normalization constant. This is nothing but the number eigenstate $|n\rangle$ given in Eq. (7) except for the prefactor. This constant C can be easily calculated by the normalization. Therefore, in the coordinate representation, the wave function is

$$\Psi_n(q) = C \int_0^{2\pi} d\eta \; e^{-in\eta} \langle q|\alpha\rangle. \tag{A13}$$

This is the exact wave function of the harmonic oscillator.

APPENDIX B: PROCEDURE OF QUANTUM COMPUTATION

In this appendix, we describe our procedure of quantum computation. Since the Hamiltonian is periodic in time, the Floquet theory can be applied. The time evolution can be reduced to evolution of the eigenstate over one driving period,

$$|\Psi(t+T)\rangle = \hat{U}(T)|\Psi(t)\rangle, \tag{B1}$$

where

$$\hat{U}(T) = \hat{U}_{\text{free}}\hat{U}_{\text{kick}} = \exp\left(-i\frac{\hat{H}_0 T}{\hbar}\right)\exp\left(-i\frac{V(\hat{q})}{\hbar}\right) \tag{B2}$$

is the Floquet operator.

To simulate quantum diffusion in this degenerate system (22), the Fourier spectral method is employed. The time interval of free propagation is divided into many slices, each having a width of Δ. For each slice the evolution operator is factored into a product of kinetic and potential propagator arranged in a symmetric way, so that a full potential step is sandwiched between two half kinetic steps, namely,

$$\exp\left(-i\frac{\hat{H}_0\Delta}{\hbar}\right) = \exp\left(-i\frac{\hat{p}^2\Delta}{4\hbar}\right)\exp\left(-i\frac{\omega_0^2\hat{q}^2\Delta}{2\hbar}\right) \times \exp\left(-i\frac{\hat{p}^2\Delta}{4\hbar}\right) + O(\Delta^3). \tag{B3}$$

This technique of symmetrically splitting the kinetic propagator reduces the error introduced by neglecting the commutator between the kinetic and potential operators. The error is reduced to $O(\Delta^3)$ from $O(\Delta^2)$ in a nonsymmetric splitting. The kinetic propagation is carried out in momentum space, since in this space the time evolution is simplified as multiplication. The potential step is performed in coordinate space for the same reason. The kick step, performed once per period, is also done in coordinate space. A fast Fourier transform routine is used to transform wave function between these two spaces.

Since the KHO model is a degenerate system, a wave packet may diffuse rapidly, even to infinity in both coordinate and momentum space. The average energy of the wave packet may reach a rather high value during the diffusion. This amplifies the error caused by the approximation made in Eq. (B3). Therefore, the self-adaptative procedure is used to adjust the time slice in Eq. (B3) in each period to make sure that the width of the time slice is much smaller than the inverse energy. Second, both coordinate and momentum spaces should be large enough. So a large number (32 768) of Fourier components are used in our computations.

[1] W. M. Zhang, J. M. Yuan, D. H. Feng, R. Qi, and J. Tjon, Phys. Rev. A **42**, 3615 (1990).

[2] W. M. Zhang, D. H. Feng, and R. Gilmore, Rev. Mod. Phys. **62**, 867 (1990).

[3] W. M. Zhang and D. H. Feng, Int. J. Mod. Phys. A **8**, 1417 (1993).

[4] W. M. Zhang and M. T. Lee (unpublished).

[5] W. M. Zhang and D. H. Feng, Phys. Rep. **252**, 1 (1995).

[6] S. T. Mo, Master's thesis, Taiwan, 1995 (unpublished).

[7] Y. Tsui and Y. Fujiwara, Prog. Theor. Phys. **86**, 443 (1991); **86**, 469 (1991).

[8] Y. Tsui, Prog. Theor. Phys. **88**, 911 (1992).

[9] A. K. Pattanayak and W. C. Schieve, Phys. Rev. Lett. **72**, 2855 (1994).

[10] A. K. Pattanayak and W. C. Schieve, Phys. Rev. E **50**, 3601 (1994).

[11] A. K. Pattanayak and W. C. Schieve, Phys. Rev. E **56**, 278 (1997).

[12] W. V. Liu and W. C. Schieve, Phys. Rev. Lett. **78**, 3278 (1997).

[13] B. Hu, B. Li, and W.-M. Zhang, e-printchao-dyn/9803004.

[14] B. V. Chirkov, Phys. Rep. **52**, 263 (1979).

[15] G. Casati, B. Chirikov, J. Ford, and F. M. Izrailev, in *Stochastic behavior in Classical and Quantum Hamiltonian Systems*, Lecture Notes in Physics Vol. 93, edited by G. Casati and J. Ford (Springer-Verlag, Berlin 1979), p. 34.

[16] D. R. Grempel, R. E. Prange, and S. Fishman, Phys. Rev. A **29**, 1639 (1984).

[17] F. L. Moore, J. C. Robinson, C. F. Bharucha, b. Sundaram, and M.G. Raizen, Phys. Rev. Lett. **75**, 4598 (1995).

[18] G. M. Zaslavsky, R. Z. Sagdeev, D. A. Usikov, and A. A. Chernikov, *Weak Chaos and Quasiregular Patterns* (Cambridge University Press, Cambridge, 1992).

[19] A. A. Chernikov, R. Z. Sagdeev, and G. M. Zaslavsky, Physica D **33**, 65 (1988).

[20] G. P. Berman, V. Yu. Rubaev, and G. M. Zaslavsky, Nonlinearity **4**, 543 (1991).

[21] F. Borgonovi and L. Rebuzzini, Phys. Rev. E **52**, 2302 (1995).

[22] D. Shepelyansky and C. Sire, Europhys. Lett. **20**, 95 (1992).

[23] I. Dana, Phys. Rev. Lett. **73**, 1609 (1994).

[24] M. Frasca, Phys. Lett. A **231**, 344 (1997).

[25] P. Kramer and M Saraceno, *Geometry of the Time-Dependent Variational Principle in Quantum Mechanics* (Springer-Verlag, Berlin, 1981).

[26] R. Jackiw and A. Kerman, Phys. Lett. A **71**, 158 (1979).

[27] M. C. Gutzwiller, *Chaos in Classical and Quantum Mechanics* (Springer-Verlag, New York, 1990).